Molecular Therapy
Nucleic Acids
Original Article

Circular RNA RBPMS inhibits bladder cancer progression via miR-330-3p/RAI2 regulation

Chen Yang,[1,2,3,4] Zezhong Mou,[1,2,4] Zheyu Zhang,[1,2,4] Siqi Wu,[1,2] Quan Zhou,[1,2] Yiling Chen,[1,2] Jian Gong,[2] Chenyang Xu,[1,2] Yuxi Ou,[1,2] Xinan Chen,[1,2] Xiyu Dai,[1,2] and Haowen Jiang[1,2,3]

[1]Department of Urology, Huashan Hospital, Fudan University, Shanghai 200040, China; [2]Fudan Institute of Urology, Huashan Hospital, Fudan University, Shanghai 200040, China; [3]National Clinical Research Center for Aging and Medicine, Fudan University, Shanghai 200040, China

Bladder cancer is a severe cancer with high mortality because of invasion and metastasis. Growing evidence has revealed that circular RNAs play critical roles in biological function, which is closely connected to proliferation and invasion of bladder cancer. In our study, we employed qRT-PCR, RNA fluorescence *in situ* hybridization (FISH), 5-ethynyl-2′-deoxyuridine (EdU), CCK-8, Transwell assays, luciferase reporter assays, xenografts, and live imaging to detect the roles of circular RNA binding protein with multiple splicing (circRBPMS) in bladder cancer (BC). Bioinformatics analysis and WB were performed to investigate the regulatory mechanism. Expression profile analysis of circular RNAs (circRNAs) in BC revealed that circRBPMS was significantly downregulated. Low circRBPMS expression correlates with aggressive BC phenotypes, whereas upregulation of circRBPMS suppresses BC cell proliferation and metastasis by directly targeting the miR-330-3p/ retinoic acid induced 2 (RAI2) axis. miR-330-3p upregulation or silencing of RAI2 restored BC cell proliferation, invasion, and migration following overexpression of circRBPMS. RAI2 silencing reversed miR-330-3p-induced cell invasion and migration as well as growth inhibition *in vitro*. Moreover, through bioinformatic analysis of the downstream target of RAI2 in the TCGA database, we identified and validated the biological role of circRBPMS through the RAI2-mediated ERK and epithelial-mesenchymal transition (EMT) pathways. We summarize the circRBPMS/miR-330-3p/RAI2 axis, where circRBPMS acts as a tumor suppressor, and provide a potential biomarker and therapeutic target for BC.

INTRODUCTION

Bladder cancer (BC) is the ninth most common cancer in the world, with a considerably varied incidence rate among different regions, genders, and ages.[1] Numerous studies suggest that circular RNA (circRNA) is related to BC progression and prognosis.[2] circRNA, a type of endogenous, non-coding, single-stranded, closed RNA, was first discovered by Sanger via electron microscope in 1976.[3] circRNA displays a loop form by ligation of the 3′ and 5′ ends and unique reverse splicing.[4] Therefore, circRNA lacks a free 5′ cap end and 3′ poly(A) tail[5] and is more stable for RNase R than linear RNA while presenting conservatism and stability.

The competitive endogenous RNA hypothesis is currently investigated the most and is a widely recognized mechanism of action.[6] Containing a large number of microRNA (miRNA) targets, circRNA can competitively combine with miRNAs as a miRNA sponge, affecting translation of mRNA by reducing the number of functional miRNAs.[7,8]

Research has demonstrated that circFNDC3B inhibits BC progression through the miR-1178-3p/G3BP2/SRC/FAK axis.[9] Although many other related studies have been conducted, the potential biological functions of circRNA in BC require further exploration. Our team has shown that silencing circUVRAG can inhibit BC growth and metastasis through the miR-223/FGFR2 axis.[10]

miRNAs are small and conserved non-coding RNAs that regulate tumor initiation and metastasis and serve as master regulators.[11,12] miRNA repress mRNA in many ways; for example, by repressing mRNA activation proteins or binding mRNA coding sequences.[13,14] Here we elaborate on the differentially expressed circRNA in BC and adjacent tumors with high-throughput sequencing technology to confirm the significant downregulation of hsa-circ-0006539 (circular RNA binding protein with multiple splicing [circRBPMS]) expression in BC, predict its potential downstream miR-330-3p and retinoic acid induced 2 (RAI2) via bioinformatics, and prove their interaction using experiments. We also summarize the relationship of circRBPMS with ERK and epithelial-mesenchymal transition (EMT) pathways and reveal that overexpressed circRBPMS can play a key role in inhibiting bladder tumor proliferation and invasion.

RESULTS

Hsa_circ_0006539 (circRBPMS) has low expression in BC

We used high-throughout sequencing to analyze the expression of circRNA in 2 pairs of BC and normal tissue samples (Table S1).

Received 12 March 2020; accepted 10 January 2021;
https://doi.org/10.1016/j.omtn.2021.01.009.

[4]These authors contributed equally

Correspondence: Haowen Jiang, Department of Urology, Huashan Hospital, Fudan University, Shanghai 200040, China.
E-mail: haowj_sh@fudan.edu.cn
Correspondence: Chen Yang, Department of Urology, Huashan Hospital, Fudan University, Shanghai 200040, China.
E-mail: yangc_huashan@163.com

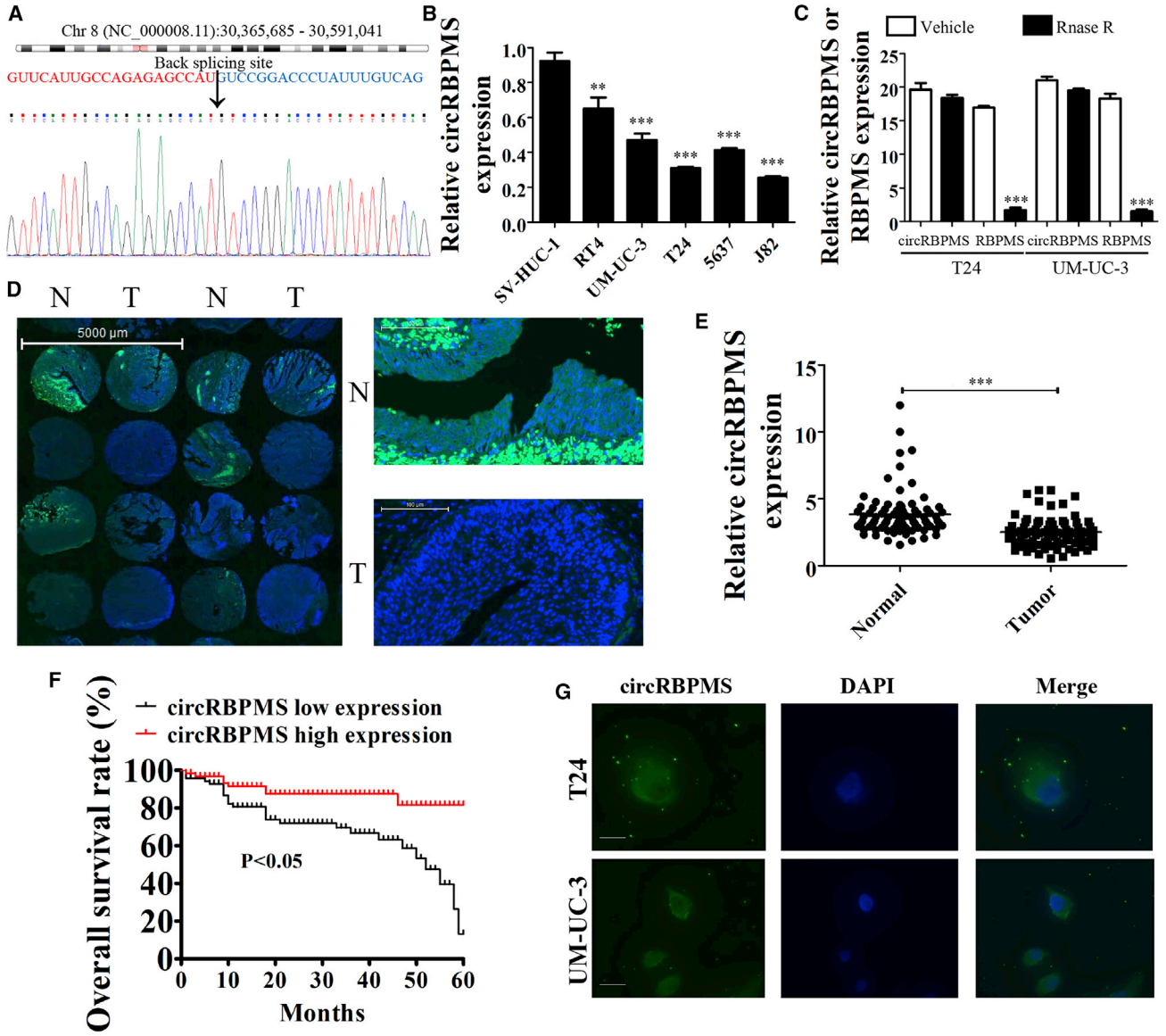

Figure 1. circRBPMS is downregulated in BC and predicts an unfavorable prognosis

(A) Genomic loci of RBPMS and circRBPMS. The schematic illustration shows that the length of circRBPMS is 331 bp. The back-splicing site is validated by Sanger sequencing. (B) Expression of circRBPMS in the normal cell line SV-HUC-1 and the bladder cancer (BC) cell lines RT4, UM-UC-3, T24, 5637, and J82, detected by qRT-PCR. Data are presented as the mean ± SD. ***$p < 0.001$, **$p < 0.01$ versus SV-HUC-1. (C) Expression of circRBPMS and linear mRNA-RBPMS treated with RNase R or left untreated was detected by qRT-PCR. circRBPMS is more resistant to RNase R than mRNA. Data are presented as the mean ± SD. ***$p < 0.001$ versus untreated samples. (D) circRBPMS is located in the cytoplasm and downregulated in BC, as detected by fluorescence *in situ* hybridization (FISH) in 90 pairs of a BC tissue microarray (TMA). (E) Relative circRBPMS expression is lower in BC, as shown by FISH values. Data are presented as the mean ± SD. ***$p < 0.001$ versus normal. (F) Prognostic significance of circRGNEF expression for individuals with BC was performed with FISH values between the circRBPMS low expression and high expression using the median value as the cutoff. The time period was 60 months. (G) FISH was used to detect the subcellular localization of circRBPMS in T24 and UM-UC-3 cells. circRBPMS was stained green, and nuclei were stained blue (DAPI). Scale bar, 20 μM.

Differential circRNA gene expression analysis identified 12 upregulated and 78 downregulated circRNAs between BCa tissues and paired normal bladder tissue ($p < 0.05$ and $|log2FC| > 2$). circRBPMS appeared to be considerably downregulated in BC derived from the RBPMS gene, with a length of 331 bp and Sanger sequencing of the unique back-splicing site of circRBPMS other than lineal RBPMS (Figure 1A); therefore, hsa_circ_0006539 is called circRBPMS. Next we tested the expression of circRBPMS in five BC cell lines (RT4, UM-UC-3, T24, 5637, and J82) using qRT-PCR. The results indicated that circRBPMS expression in the T24 and UM-UC-3 cell lines was

Table 1. Relationship between the expression levels of circRBPMS and clinicopathological features in BC

		circRBPMS expression		
Characteristics	No. (%)	Low (%)	High (%)	p value
Gender				
Male	81 (90.0)	46 (56.8)	35 (43.2)	1.000
Female	9 (10.0)	5 (55.6)	4 (44.4)	
Age				
<65	56 (62.2)	36 (64.3)	20 (35.7)	0.080
≥65	34 (37.8)	15 (44.1)	19 (55.9)	
Tumor size				
<3 cm	38 (42.2)	16 (42.1)	22 (57.9)	0.020
≥3 cm	52 (57.8)	35 (67.3)	17 (32.7)	
Clinical stage				
Ta–T1	44 (48.9)	18 (40.9)	26 (59.1)	0.005
T2–T4	46 (51.1)	33 (71.7)	13 (28.3)	
Grade				
Low	51 (56.7)	26 (51.0)	25 (49.0)	0.284
High	39 (43.3)	25 (64.1)	14 (35.9)	
Lymphatic metastasis				
Yes	22 (24.4)	17 (77.3)	5 (22.7)	0.028
No	68 (75.6)	34 (50.0)	34 (50.0)	
Muscle invasion				
NMIBC	61 (67.8)	29 (47.5)	32 (52.5)	0.013
MIBC	29 (32.2)	22 (75.9)	7 (24.1)	
Total	90	51	39	

somewhat decreased in comparison with normal SV-HUC-1 cells (Figure 1B). By treating T24 and UM-UC-3 cells with RNase R, we found that circRBPMS was more resistant than its linear counterpart (Figure 1C), as expected. Then we used 90 pairs of human BC samples and adjacent samples to carry out RNA fluorescence *in situ* hybridization (FISH) assays and verified that circRBPMS was mainly localized in the cytoplasm (Figure 1D) and less expressed in BC tissues than in adjacent normal tissues (Figure 1E). As shown in Table 1, we also discovered that low circRBPMS expression was positively correlated with tumor size, clinical stage, lymphatic metastasis, and muscle invasion. In addition, several recent studies have shown that differential expression of circRNA contributes greatly to the prognosis of individuals with BC;[15,16] those who exhibit low expression of circRBPMS are associated with a worse prognosis in contrast to those with high expression (Figure 1F). Furthermore, circRBPMS was mainly present in the cytoplasm (Figure 1G) in T24 and UM-UC-3 cells, as shown by RNA FISH of circRBPMS, which revealed a potential role of mediating downstream biological roles.

Overexpression of circRBPMS suppressed cell proliferation and invasion *in vitro*

To further investigate the effects of circRBPMS on BC cells, we constructed a lentiviral overexpression vector (LV-circRBPMS). qRT-PCR analysis proved that transfection of LV-circRBPMS can increase the expression of circRBPMS in T24 and UM-UC-3 cells (Figure 2A). CCK-8 assays confirmed that high levels of circRBPMS can inhibit proliferation of T24 and UM-UC-3 cells (Figures 2B and 2C). Flow cytometry assays showed that S phase was decreased, whereas G0/G1 phase proportions were increased. We also observed a sub-G0 peak following overexpression of circRBPMS, indicating apoptosis (Figure 2D).[17] The apoptosis rates of circRBPMS-overexpressing T24 and UMUC-3 cells increased as expected, which would account for cell phenotype alteration as proliferation and migration (Figure 2E). Overexpression of circRBPMS suppressed closure of scratch wounds (Figure 2F; Figures S1A and S1B), suggesting that circRBPMS plays an important role in BC cell invasion. Colony formation assays and 5-ethynyl-2′-deoxyuridine (EdU) assays also revealed that overexpression of circRBPMS can suppress proliferation of tumor cells (Figures 2G and 2H; Figures S1C and S1D).

Overexpression of circRBPMS decreased BC cell proliferation and metastasis *in vivo*

It was also found in xenograft assays that circRBPMS overexpression could inhibit tumor size (Figure 3A), tumor volume (Figure 3B), and tumor weight (Figure 3C), as measured against negative control (NC) cells. Immunohistochemistry detection with Ki67 staining demonstrated that overexpressed circRBPMS suppresses Ki67 expression in tumor tissue (Figure 3D), indicating that circRBPMS suppresses tumor growth. Transwell assays showed that overexpression of circRBPMS inhibits migration of T24 and UM-UC-3 cells (Figure 3E). Furthermore, we injected luciferase (luc)-labeled T24 cells containing overexpression of LV-circRBPMS and LV-NC into mice via the tail vein, and live imaging after 21 days showed a reduction of visible lung metastasis sites. These results suggest that overexpressed circRBPMS suppresses tumor metastasis *in vivo* (Figure 3F).

circRBPMS inhibits miRNA expression, serving as an RNA sponge for miR-330-3p

Bioinformatics play a crucial role in predicting downstream targets of circRNA.[18] We drew a schematic diagram of the potential miRNA might be combined which predicted by Encori, CircInteractome, and circMIR (Figures 4A and 4B). miR-330-3p has been shown to be downregulated in various tumors, such as breast cancer[19], non-small cell lung cancer,[20] and osteosarcoma.[21] However, miR-330-3p is also upregulated in cancer tissue, which inhibits cell viability and invasion.[22] To better detect the potential downstream target of circRBPMS, we conducted an RNA pull-down assay and found that only miR-330-3p could be pulled down by the circRBPMS probe (Figure 4C). Ago2 RNA immunoprecipitation (RIP) was applied to further validate the interaction between circRBPMS and miR-330-3p; higher circRBPMS and miR-330-3p levels were observed in anti-Ago2 RIP than in anti-immunoglobulin G (IgG) RIP (Figure 4D). To future confirm the expression and biological role of miR-330-3p in BC, significantly higher expression of miR-330-3p was observed in five BC cell lines (RT4, UM-UC-3,

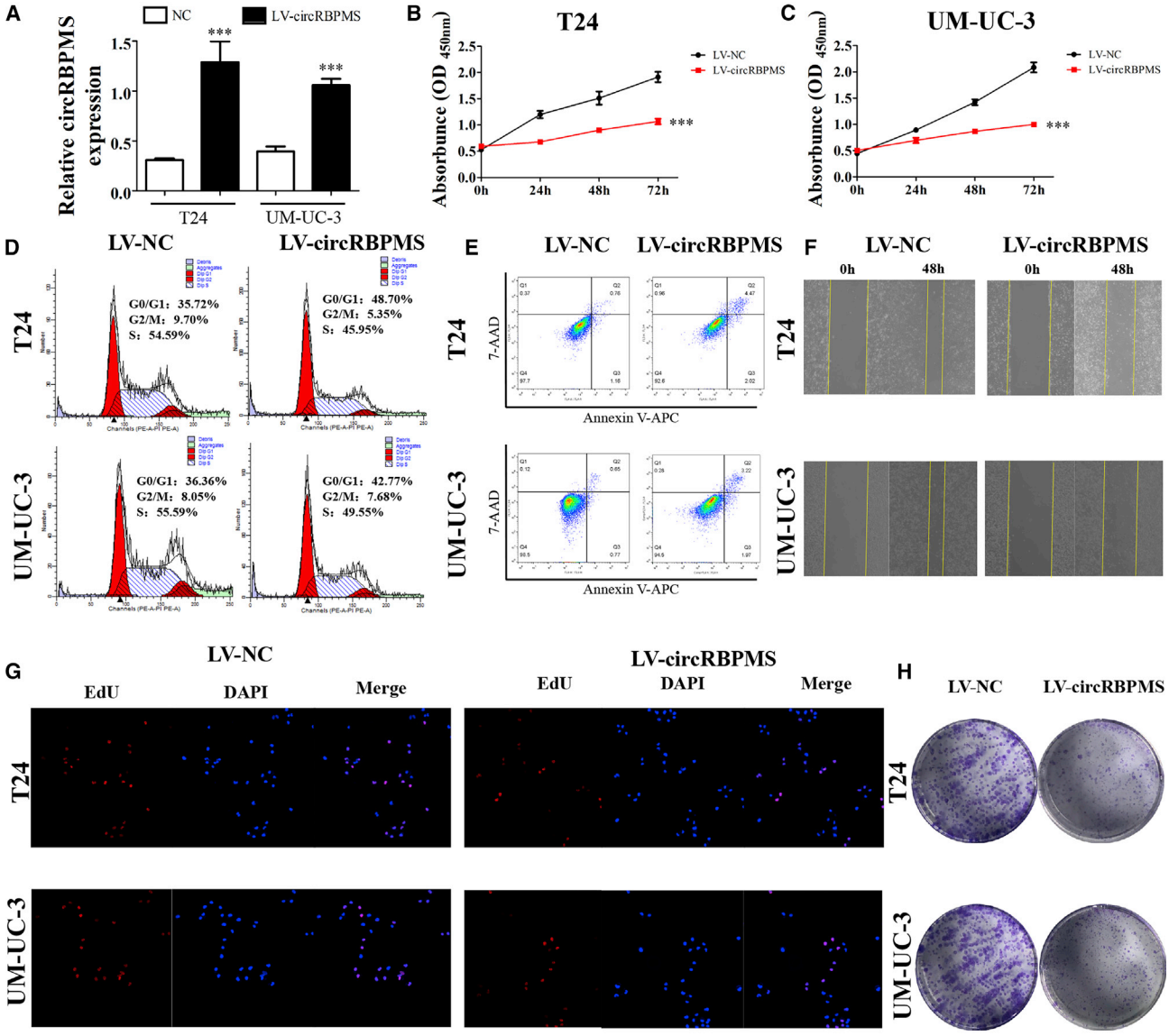

Figure 2. Overexpression of circRBPMS suppressed BC cell proliferation *in vitro*

(A) The efficiency of LV-circRBPMS overexpression compared with a negative control (NC) in T24 and UM-UC-3 cells was detected by qRT-PCR. Data are presented as the mean ± SD. ***$p < 0.001$ versus NC. (B and C) CCK-8 proliferation assays of T24 and UM-UC-3 were detected to preform the proliferation of LV-circRBPMS and NC. Data are presented as the mean ± SD. ***$p < 0.001$ versus NC. (D) Flow cytometry was used to measure the cell cycle distribution of LV-circRBPMS and NC in T24 and UM-UC-3 cells separately after PI staining. (E) Apoptosis rates of LV-circRBPMS and NC in T24 and UM-UC-3 were detected by Annexin V-7-AAD staining and analyzed by flow cytometry. (F) Wound healing assays for T24 and UM-UC-3 cells transfected with LV-circRBPMS and LV-NC were performed for 48 h to detect cell migration ability. (G) The proliferation ability of T24 and UM-UC-3 cells transfected with LV-circRBPMS and LV-NC was detected by EdU assay. (H) A colony formation assay was performed to detect the colony formation ability of T24 and UM-UC-3 cells transfected with LV-circRBPMS and LV-NC.

T24, 5637, and J82) compared with SV-HUC-1 cells (Figure S2A) and in 42 pairs of BC tissue compared with normal tissue, as shown by qRT-PCR (Figure S2B). Furthermore, TCGA expression profiles also demonstrated higher expression of miR-330-3p in BC samples (Figure S2C). miR-330-3p could inhibit proliferation of T24 and UM-UC-3 cells, and this phenotype could be reversed by inhibiting miR-330-3p (Figures S2D and S2E) in CCK-8 assays. The interaction detected by RNA FISH in T24 and UM-UC-3 cells revealed that circRBPMS and miR-330-3p were co-expressed in the cytoplasm (Figure 4E). We constructed dual-luc reporter vectors that contained wild-type (WT) and mutated (Mut) circRBPMS sequences capable of binding miR-330-3p (Figure 4F) to confirm

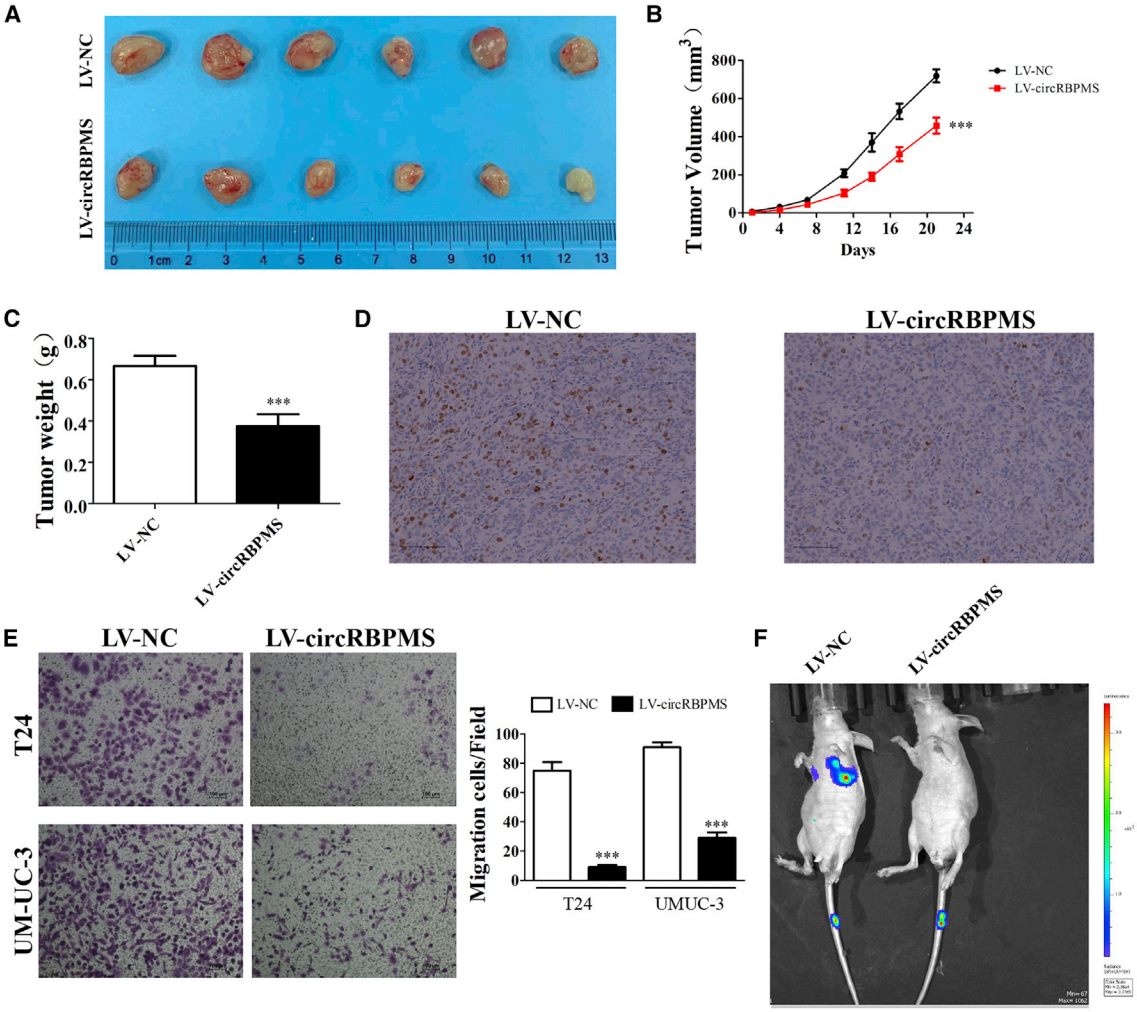

Figure 3. circRBPMS overexpression suppressed BC cell proliferation and metastasis *in vitro*

(A) Tumor sizes were measured and compared for LV-NC-T24 and LV-circRBPMS-T24 xenografts in nude mice after 21 days. (B and C) Tumor volume and weight were measured separately. Data are presented as the mean ± SD. ***$p < 0.001$ versus NC. (D) Ki-67 staining section of relative tumor tissue. Scale bar, 100 μM. (E) The invasion ability of T24 and UM-UC-3 cells was detected using separate Transwell assays. ***$p < 0.001$ versus NC. (F) The metastasis ability of LV-NC-T24-luc and LV-circRBPMS-T24-luc by intravenous tail injection was detected using live imaging.

the interaction between circRBPMS and miR-330-3p. After transfecting vectors to HEK293T cells that did or did not contain a miR-330-3p mimic and circRBPMS, dual-luciferase assays showed that miR-330-3p suppressed luc activity in WT cells but not in Mut cells (Figure 4G). All of this evidence indicates that miR-330-3p is a direct downstream target of circRBPMS and serves as a cancer promoter in BC.

miR-330-3p works as a mRNA suppressor to inhibit RAI2 expression

We took advantage of the databases miRWalk, miRDB, TargetScan, and Encori and differentially expressed gene analysis via the R package of BC in TCGA to predict potential downstream target genes of miR-330-3p (Figure 5A). Cytoscape software was used to draw the ceRNA network (Figure 5B). RAI2, one of the predicted targets, attracted our attention because of its reported tumor-suppressive biological function. RAI2 can inhibit early metastatic spread of estrogen receptor-positive breast cancer as a differentiation factor.[23] We further validated that transfection with a miR-330-3p mimic decreased RAI2 levels in T24 and UMUC-3 cells, whereas a miR-330-3p inhibitor had the opposite effect (Figures S3A and S3B). However, the role of RAI2 in BC largely remains unknown. We used the GEPIA database (http://gepia.cancer-pku.cn/detail.php) to summarize expression of the RAI2 gene in 404 BC and 28 control samples and discovered that it was significantly less expressed in BC (Figure 5C). RAI2 expression in 42 pairs of BC tissue and normal tissue

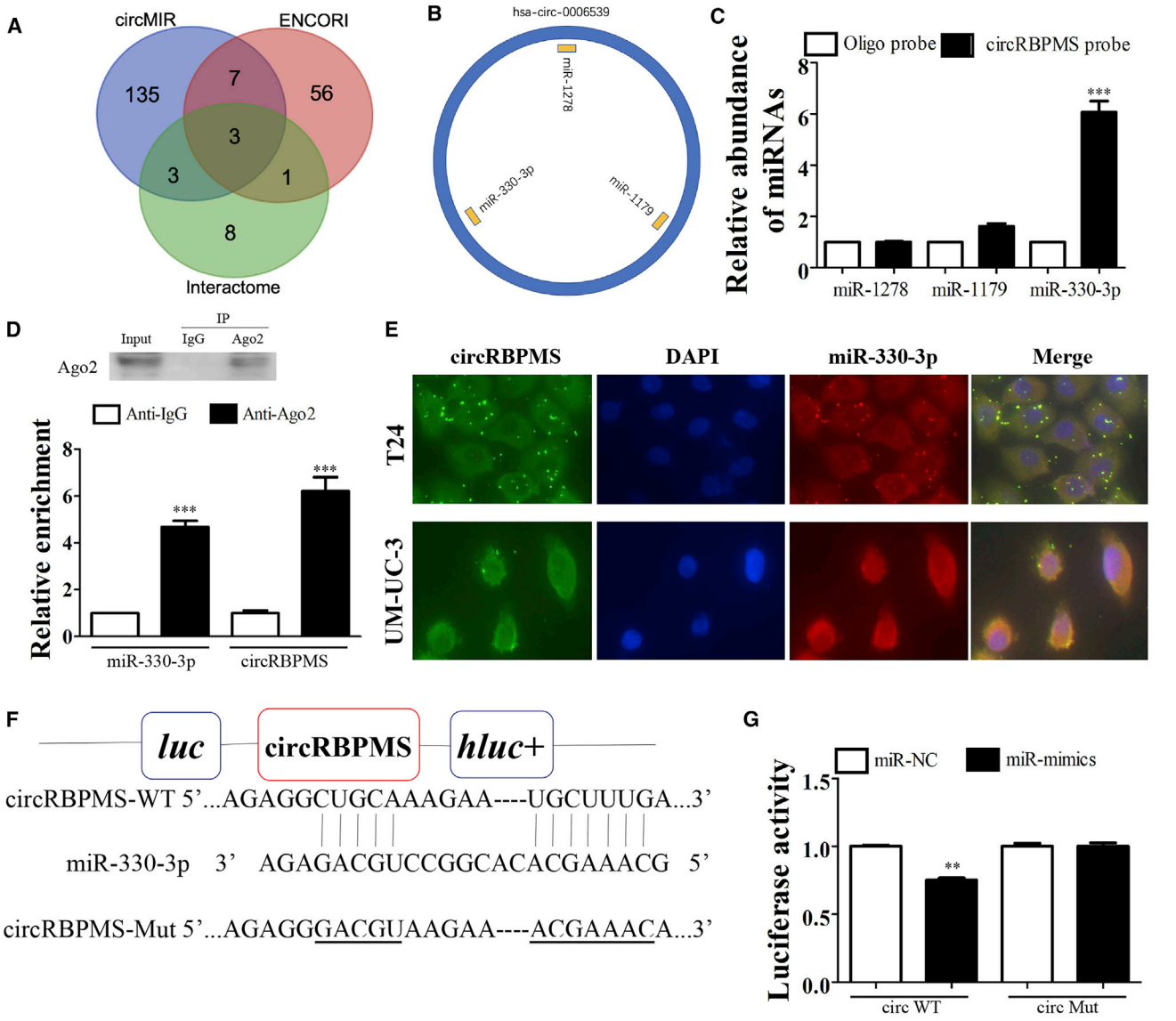

Figure 4. circRBPMS is a sponge of miR-330-3p in BC cells

(A and B) Venn diagram of miR-330-3p, miR-1278, and miR-1179, predicted by the Encori, Circular RNA, CircInteractome databases and the software circMIR, shown as a schematic illustration. (C) RNA pull-down was performed to evaluate the affinity of circRBPMS for miR-330-3p in T24 cells. Relative miRNA expression under the enriched of circRBPMS probe which detected by qRT-PCR. Data are presented as the mean ± SD. ***$p < 0.001$. (D) RIP experiments were performed in T24 cells against IgG or Ago2, and the precipitated circRBPMS and miR-330-3p were detected by qRT-PCR. ***$p < 0.001$ versus IgG. (E) FISH shows the subcellular location of miR-330-3p and circRBPMS. Nuclei were stained with DAPI. circRBPMS was stained green (cy3), nuclei were labeled blue (DAPI), and miR-330-3p was labeled red (cy5). Scale bar, 20 μM. (F) Dual-luc reporter assays show the binding properties of circRBPMS and miR-330-3p. The mutated (Mut) version of circRBPMS is also shown. (G) Relative luc activity was determined 48 h after transfection with miR-330-3p mimic/normal control or with the circRBPMS WT/Mut in HEK293T cells. Data are presented as the mean ± SD. **$p < 0.01$.

also showed significantly decreased expression in BC tissue (Figure 5D). miR-330-3p could reduce the expression of RAI2, and overexpression of circRBPMS could increase the level of RAI2, and cells co-transfected with circRBPMS and the miR-330-3p mimic could reverse RAI2 overexpression in T24 and UM-UC-3 cells (Figure 5E). We also constructed dual-luc reporter vectors that contained WT and Mut RAI2 sequences capable of binding miR-330-3p (Figure 5F). Dual-luc assays showed that miR-330-3p suppressed luc activity in WT cells but not in Mut cells (Figure 5G), which indicated that RAI2 is the downstream target of miR-330-3p. To conclude, circRBPMS increases expression of RAI2 by working as a miR-330-3p sponge.

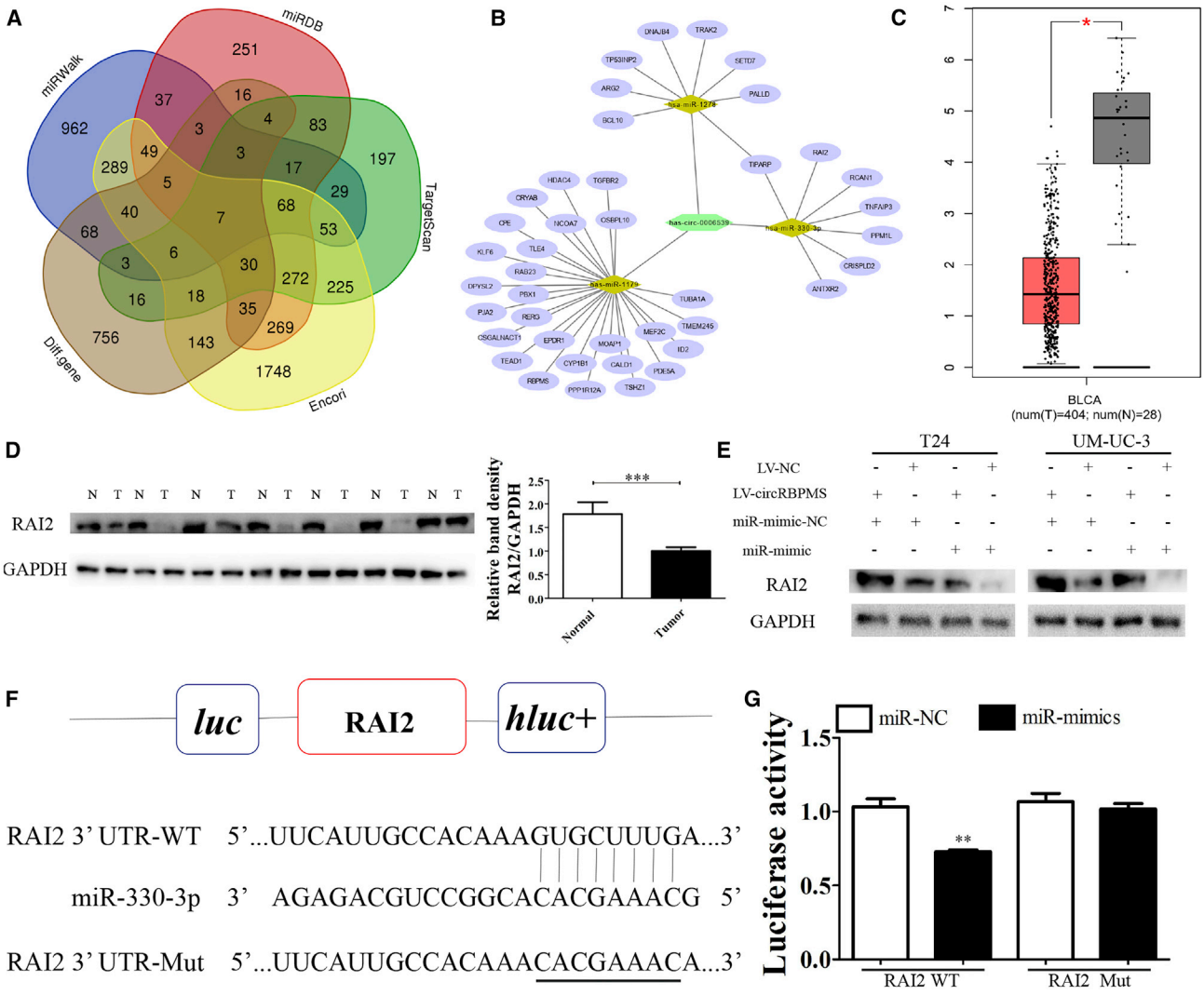

Figure 5. miR-330-3p is a direct target of RAI2 in BC cells

(A) Venn diagram of predicted downstream mRNA from miRWalk, miRDB, TargetScan, Encori, and TCGA regulated by miR-330-3p. (B) circRBPMS-miR-330-3p-RAI2 ceRNA network drew by Cyctoscape software. (C) Down-expression of RAI2 in BC tissue versus normal tissue was analyzed by GEPIA database. *p < 0.05. (D) Expression of RAI2 in BC was further validated in 42 pairs of BC tissues. GAPDH was regarded as endogenous control. Relative expression of RAI2 was analyzed with ImageJ. Data are presented as the mean ± SD. **p < 0.01. (E) Western blot showed RAI2 levels among LV-circRBPMS+miR-NC, LV-NC+miR-NC, LV-circRBPMS+miR-330-3p, and LV-NC+miR-330-3p both in T24 and UM-UC-3. (F) Dual-luc reporter assays showed binding properties of miR-330-3p and RAI2. The Mut version of the 3′UTR-RAI2 is also shown. (G) Relative luc activity was determined 48 h after transfection with the miR-330-3p mimic/normal control or with the 3′ UTR-RAI2 WT/Mut in HEK293T cells. Data are presented as the mean ± SD. **p < 0.01.

miR-330-3p overexpression or RAI2 silencing restored proliferation, migration, and invasion after circRBPMS overexpression

Of three shRNA sequences targeting RAI2, shRAI2-3 shows the highest inhibitory effect on expression of RAI2 in T24 and UM-UC-3 cells (Figures S3C and S3D). shRAI2-3 of T24 and UM-UC-3 cells also show the highest cell proliferation rate (Figures S3E and S3F). Thus, we chose shRAI2-3 to further verify the correlation of circRBPMS/miR-330-3p/RAI2 by detecting RAI2 expression in the LV-NC group, LV-circRBPMS group, LV-circRBPMS + shRAI2 group, and LV-circRBPMS + mimic group. The results demonstrated that high levels of circRBPMS increase RAI2 expression, whereas shRAI2 had the opposite effect. The use of a mimic can ameliorate this expression, but the expression level was still lower than that of the circRBPMS-overexpressing group alone (Figure 6A). Then we performed CCK-8 assays and colony formation assays to investigate the effects on cell proliferation *in vitro*. Both indicated that, in the case of circRBPMS overexpression, inhibiting RAI2 or overexpressing miR-330-3p can promote proliferation of tumors (Figures 6B and 6C). Transwell assays revealed that overexpression of circRBPMS

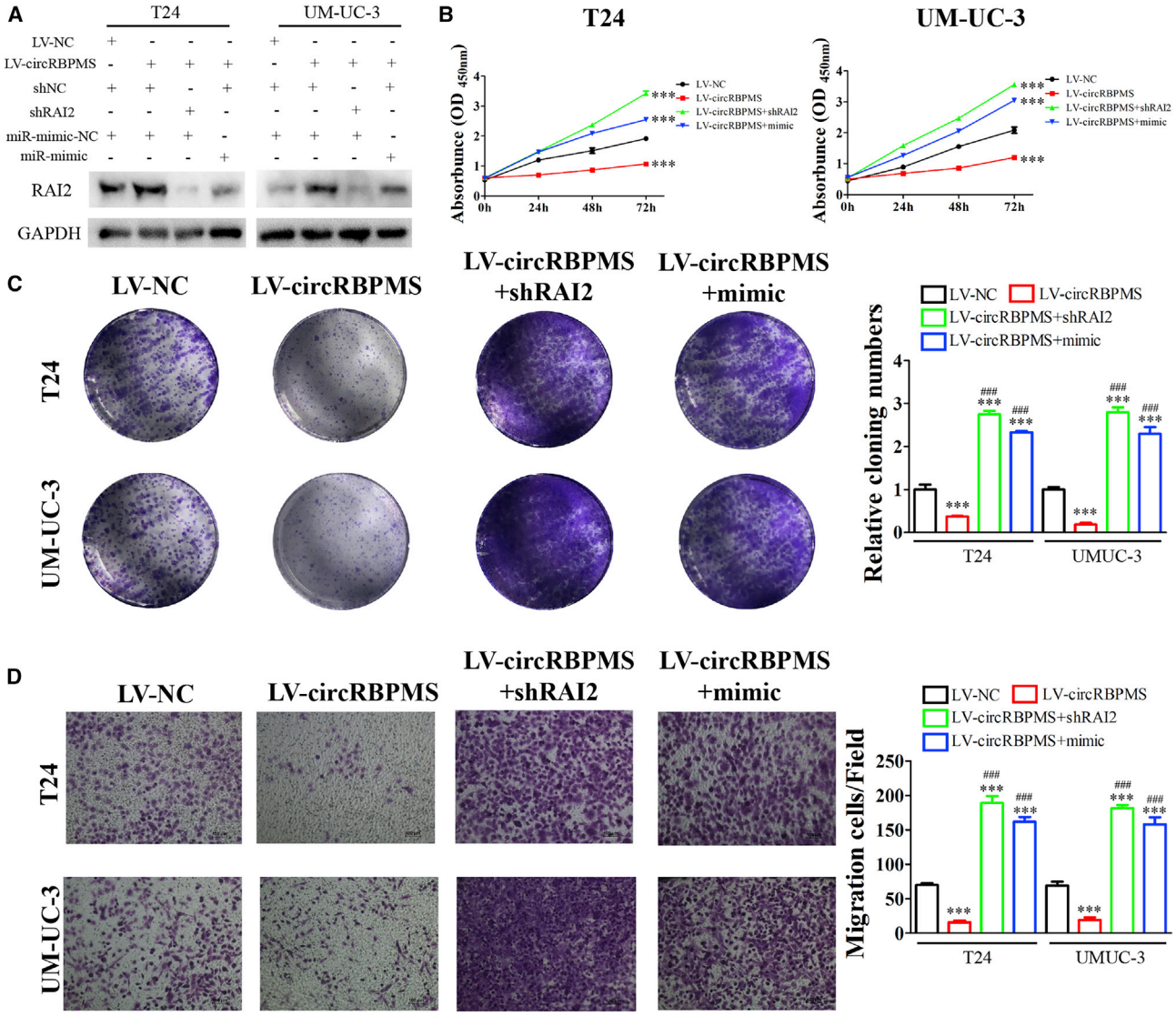

Figure 6. Overexpression of miR-330-3p or RAI2 silencing restored proliferation, migration, and invasion after circRBPMS overexpression

(A) Expression of RAI2 in T24 and UM-UC-3 cells was detected by western blot for the NC, circRBPMS overexpression, circRBPMS overexpression with RAI2 silencing, and circRBPMS overexpression with miR-330-3p. GAPDH was used as an endogenous control. (B and C) The proliferation ability of NC, circRBPMS overexpression, circRBPMS overexpression with RAI2 silencing, and circRBPMS overexpression with miR-330-3p was detected by CCK-8 assays and colony formation assays. Data are presented as the mean ± SD. ***p < 0.001 versus LV-NC, ###p < 0.001 versus LV-circRBPMS. (D) The migration and invasion ability of NC, circRBPMS overexpression, circRBPMS overexpression with RAI2 silencing, and circRBPMS overexpression with miR-330-3p was detected by Transwell assays. ***p < 0.001 versus LV-NC, ###p < 0.001 versus LV-circRBPMS.

inhibited cell migration and invasion, whereas RAI2 silencing or miR-330-3p upregulation reversed the situation (Figure 6D).

RAI2 silencing restored proliferation, migration, and invasion after miR-330-3p downregulation

To further explore the relationship between miR-330-3p and RAI2, we detected RAI2 expression after inhibiting miR-330-3p and both miR-330-3p and shRAI2 on T24 and UM-UC-3p, respectively. The results revealed that expression of RAI2 increased after inhibiting miR-330-3p, whereas shRAI2 could degrade miR-330-3p-mediated overexpression of RAI2, which suggested that miR-330-3p had a direct inverse effect on downstream RAI2 (Figure 7A). Silencing miR-330-3p could inhibit proliferation of T24 and UM-UC-3 cells, but this could be reversed after adding shRAI2 (Figures 7B and C). Moreover, miR-330-3p inhibited migration and invasion of T24 and UM-UC-3 cells, and this could also be reversed after adding

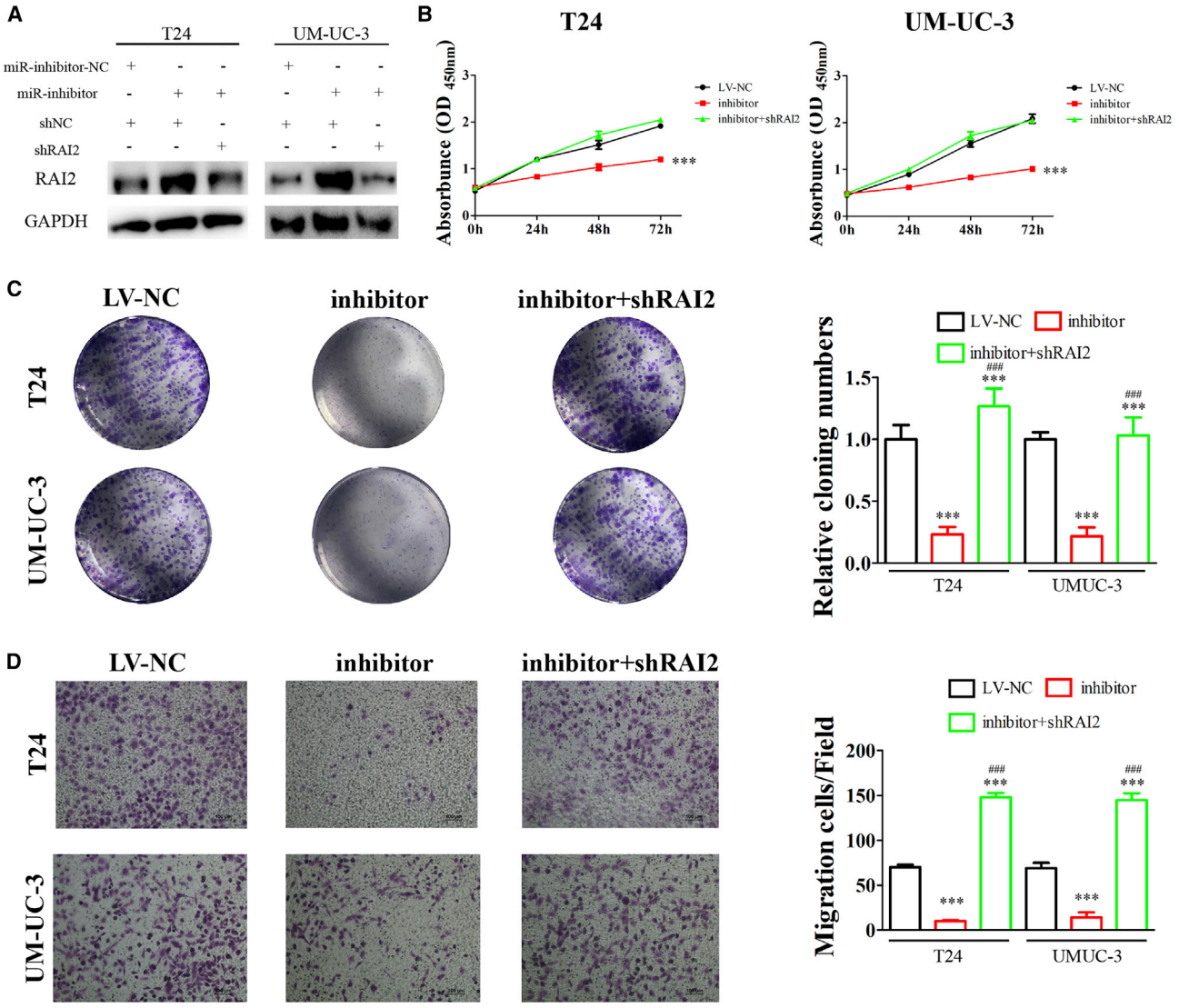

Figure 7. RAI2 silencing restored proliferation, migration, and invasion after miR-330-3p downregulation

(A) Expression of RAI2 in T24 and UM-UC-3 cells was detected by western blot for the NC, miR-330-3p inhibitor, and miR-330-3p inhibitor with RAI2 silencing. GAPDH was used as an endogenous control. (B and C) The proliferation ability of the NC, miR-330-3p inhibitor, and miR-330-3p inhibitor with RAI2 silencing was detected by CCK-8 assays and colony formation assays. Data are presented as the mean ± SD. ***$p < 0.001$ versus LV-NC, ###$p < 0.001$ versus inhibitor. (D) The migration and invasion ability of the NC, miR-330-3p inhibitor, and miR-330-3p inhibitor with RAI2 silencing was detected by Transwell assays. ***$p < 0.001$ versus LV-NC, ###$p < 0.001$ versus inhibitor.

shRAI2 in Transwell assays, which showed the same trend as above (Figure 7D).

circRBPMS inhibits the EMT and ERK pathways through RAI2

We proceed to discover the underlying downstream pathway of circRBPMS-mediated RAI2 through gene set enrichment analysis. KRAS-ERK signaling, myogenesis, UV response, and EMT processes attracted our attention among all outcomes that had a statistically significant difference (Figure 8A). We further validated pathway-related proteins of EMT (E-Cadherin and Vimentin), KRAS-ERK (p-ERK and ERK), myogenesis (Myf5 and MyoG), and UV response (GADD45A and GAL1) in circRBPMS-overexpressing T24 and UM-UC-3 cells (Figure 8B) and xenograft T24 tumors (Figure 8C). The results showed that E-cadherin and p-ERK were upregulated but vimentin was downregulated under circRBPMS overexpression, which indicated that the EMT and KRAS/ERK pathways are involved in circRBPMS overexpression in BC. A schematic diagram showing the biological function of the circRBPMS/miR-330-3p/RAI2/EMT-ERK pathway in inhibiting BC cell proliferation and metastasis is shown in Figure 8D.

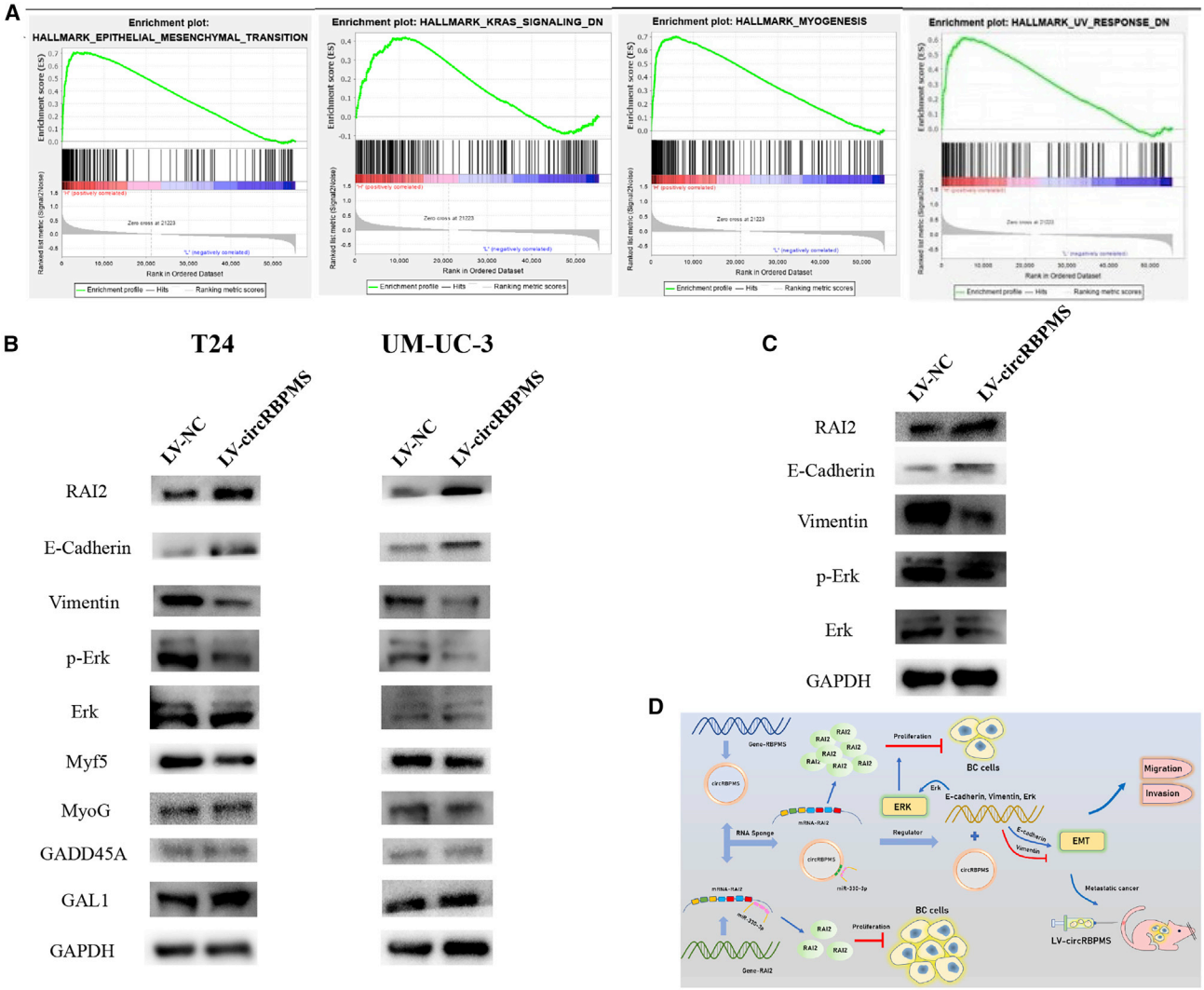

Figure 8. circRBPMS performs its biological role through the EMT and KRAS-ERK pathways

(A) Four potent relevant pathways were obtained by GSEA of BC in the TCGA database. (B) Western blot was performed to detect the core protein expression of 4 pathways in T24 and UM-UC-3 cells transfected with LV-circRBPMS or left untransfected. GAPDH was used as an endogenous control. (C) Western blot was performed to detect the expression of related proteins of the EMT and ERK pathways in LV-NC-T24 and LV-circRBPMS-T24 xenograft tumors. GAPDH was used as an endogenous control. (D) Schematic diagram showing the inhibitory effect of circRBPMS on BC cell proliferation and metastasis by impeding the miR-330-3p/RAI2 interaction-mediated EMT and ERK pathways.

DISCUSSION

Previous studies indicate that after circRNA is generated, it is transmitted to the cytoplasm and perform biological functions;[24] this process was proven by RNA FISH luc experiments. Bioinformatics technology advanced research and exploration of circRNAs.[25] As described previously, circRNAs perform biological functions in various ways; for example, by acting as RNA sponges, combining RBPs, and serving as encoding sequences.[26] The RNA sponge mechanism is discussed the most; a large number of circRNAs contain only few miRNA binding sites, so it is difficult for them to function as miRNA sponges.[27] However, it has been demonstrated by RNA pull-down assays that circRBPMS can regulate protein expression as RNA sponges because of their miRNA binding targets (CUGCAAAGAA—UGCUUUGA). Many studies indicate that circRNAs are widely expressed in human tissue such as the cardiovascular system[28] and closely related to non-tumor diseases such as Parkinson's disease,[7], Alzheimer's disease,[29] and myotonic dystrophy.[30] Recently, circRNAs have been revealed to participate in the occurrence and growth of tumors, including highly expressed ones.[31] Hence, by inhibiting the working patterns of circDOCK1/hsa-miR-132-3p/Sox5, we can suppress BC cells and restrain their proliferation and migration.[32] We observed significant inhibition of proliferation and

induction of apoptosis in BCa cells with circRBPMS overexpression, and those account for cell invasion, migration and metastasis. Recurrence and metastasis remain two fundamental factors affecting the prognosis of individuals with BC, so it is important to understand the role of circRNA in regulation of BC recurrence and metastasis. Through comparative research of highly invasive BC and lowly invasive BC, low expression of circZKSCAN1 was positively correlated with poor remission of BC as well as a high recurrence rate and tumor metastasis.[33] We constructed LV-circRBPMS and explored its invasion ability using Transwell assays, where live imaging indicated that circRBPMS suppressed metastasis *in vivo* after intravenous tail injection. We effectively proved that circRBPMS can inhibit invasion and metastasis of BC cells. circRBPMS is downregulated significantly in BCa tissue and cells, and m6A methylation[34] and RNA splicing factors[35] can regulate formation of specific circRNAs, accounting for the downregulation of circRBPMS in BCa. Several studies have demonstrated a distinct mechanism of circRNA for regulating its parental gene.[36,37] RBPMS serves as the parental gene for circRBPMS, performing RBP biofunctions, whereas the circRNA forms through an RBP-driven circularization mechanism,[38] which indicates that further work should focus on discovering the regulatory roles of circRBPMS and RBPMS.

As a cancer-promoting miRNA, miR-330-3p contributes greatly to generation and growth of tumors, such as gastric cancer, liver cancer, colorectal cancer, and breast cancer.[19,39–41] Researches on miR-330-3p in urinary tumors remains insufficient, so it is crucial to analyze the mechanism of miR-330-3p in BC. Cohort studies have shown that expression of miR-330-3p is related to the prognosis of individuals with invasive breast cancer,[41] which agrees with our finding that overexpression of miR-330-3p enhances BC cell migration and invasion. We predicted three possible downstream binding targets and confirmed, via qRT-PCR, that miR-330-3p is a potential target of circRBPMS.

As a member of the retinoic acid family, RAI2 may affect the body development process and cell growth and differentiation.[23] RAI2 is generally believed to be a novel tumor suppressor for various cancers, including colorectal cancer[42] and breast cancer;[43] however, there is no proof for a relationship between RAI2 and BC. After comparing the expression of RAI2 in the TCGA database of 404 BC samples and 28 normal samples on GEPIA site, we discovered that RAI2 was significantly downregulated in BC. Our experiments demonstrated that overexpression of RAI2 could considerably suppress proliferation, migration, and invasion of BC cells, which is consistent with previous research results, so RAI2 is of great importance in BC migration and invasion. To further determine the relevant pathways, we analyzed RAI2-related pathways using GSEA. Of all of these potential pathways, the relationship with EMT attracted our attention. EMT is a process whereby epithelial cells lose their previous characteristics and acquire novel mesenchymal features, which is closely connected with the occurrence, development, and metastasis of cancers.[44] Western blot results indicated that circRBPMS downregulates the expression of Vimentin to inhibit the EMT process. Therefore, we speculated that circRBPMS could affect EMT by inhibiting the ERK pathway. Our western blot assays also confirmed our previous inference that circRBPMS can inhibit expression of p-ERK, a marker of ERK pathway activation.

In summary, we confirmed that circRBPMS can inhibit the occurrence and development of BC. Downstream targets were predicted via bioinformatics analysis and then proven experimentally. We demonstrated the working patterns of circRBPMS/miR-330-3p/RAI2 whereby miR-330-3p can be absorbed by a sponge so that inhibition of RAI2 can be reduced. Migration and invasion of BC cells were inhibited by suppression of the ERK pathway and then by the process of EMT. Thus, our study provides a new diagnostic and therapeutic target for BC treatment.

MATERIALS AND METHODS

Cell lines

The SV-HUC-1 and BC (RT4, UM-UC-3, T24, 5637, and J82) cell lines were purchased from the Type Culture Collection (Shanghai, China) at the Chinese Academy of Sciences. SV-HUC-1 was cultured in Ham's F-12K medium (Gibco). T24 and J82 cells were cultured in Dulbecco's modified Eagle's medium (Gibco). 5637 and UM-UC-3 cells were cultured in 1640 medium (Gibco). All cells were cultured in medium supplemented with 10% fetal bovine serum (FBS). All cells were cultured in a humidified incubator with 5% CO_2, 100 units/mL penicillin, and 100 μg/mL streptomycin.

Samples

A total of 90 pairs of BC tissue and adjacent normal tissue (Huashan cohort 1) were collected from individuals with BC who received surgical treatment in Huashan Hospital, Fudan University between January 2007 and January 2013, including a 5-year follow-up. Another 42 pairs of BC tissue and adjacent normal tissue (Huashan cohort 2) were collected from individuals with BC who received surgical treatment in Huashan Hospital, Fudan University between January 2018 and January 2020. None of the individuals received any preoperative local or systemic treatment before specimen collection. Written informed consent was acquired from the participants or their relatives, and the project was approved by the Board and Ethics Committee of Huashan Hospital, Fudan University. The collected tissues were directly deposited in liquid nitrogen and 4% paraformaldehyde until further use. Two experienced pathologists confirmed the histological and pathological diagnoses of BC according to the 7th edition of the TNM classification of the International Union Against Cancer (UICC, 2009).

RNA FISH

Specific probes for hsa_circ_0006539 (circRBPMS) (Bio-5′-AAATAGGGTCCGGACATGGCTCTCTGGCAA-3′-Bio) and probes against miR-330-3p (Dig-5′-TCTCTGCAGGCCGTGTGCTTTGC-3′-Dig) were prepared (Geneseed Biotech, Guangzhou, China). The signals were detected by Cy3-conjugated anti-digoxin and fluorescein isothiocyanate (FITC)-conjugated anti-biotin antibodies (Jackson ImmunoResearch Laboratories, West Grove, PA, USA). Cell nuclei

were counterstained with DAPI. Finally, images were obtained on an LSM 700 confocal microscope (Carl Zeiss, Oberkochen, Germany). Tissue sections were examined using an Olympus FluoView FV1000 confocal microscope (Olympus, London, UK) and photographed with a digital camera.

RNase R treatment

Total RNA extracted from T24 and UMUC-3 cells was treated with RNase R (Epicenter Technologies, USA) according to the manufacturer's instructions for 30 min at 37°C. The stability of circRBPMS and RBPMS mRNA was analyzed by qRT-PCR.

RNA extraction and qRT-PCR

Total RNA was extracted with TRIzol reagent (Invitrogen) according to the manufacturer's protocol. Reverse transcription was performed by using a PrimeScriptTMRT Reagent Kit (TaKaRa) to obtain cDNA. The cDNA was subjected to quantitative real-time PCR on an ABI 7900HT sequence detection machine (Thermo Fisher Scientific). The $2^{-\Delta\Delta CT}$ method was used to calculate differences in expression. GAPDH was used as the control gene for circRNA and mRNA. U6 was used as an internal control for the level of miRNA expression.

The primers were as follows:

GAPDH forward: 5′-CAAGGCTGAGAACGGGAAG-3′

GAPDH reverse: 5′-TGAAGACGCCAGTGGACTC-3′

RBPMS forward: 5′-CATTGCCAGAGAGCCATATGAG-3′

RBPMS reverse: 5′-AGGTGAAAGCAGGAGGAGGTA-3′

circRBPMS forward: 5′-TTAAGGGCTATGAGGGTT-3′

circRBPMS reverse: 5′-GTGTTGGGCAGAGGAGTA-3′

U6 forward: 5′-CTCGCTTCGGCAGCACA-3′

U6 reverse: 5′-AACGCTTCACGAATTTGCGT-3′

hsa-miR-1278 forward: 5′-ACACTCCAGCTGGGTAGTACTGTGCATATC-3′

hsa-miR-1179 forward: 5′-ACACTCCAGCTGGGAAGCATTCTTTCATT-3′

hsa-miR-330-3p forward: 5′-ACACTCCAGCTGGGGCAAAGCACACGGCCTG-3′

miRNA reverse: 5′-TGGTGTCGTGGAGTCG-3′

Bioinformatics analysis

Bioinformatics analysis was used to predict the potential downstream targets of circRBPMS. We used the databases Encori (http://starbase.sysu.edu.cn) and CircInteractome (http://circinteractome.nia.nih.gov/) and the software circMIR to predict the three potential downstream miRNAs: miR-1278, miR-1179, and miR-330-3p. We used the R package to analyze the differentially expressed gene download from the TCGA database. We also used miRWalk (http://mirwalk.umm.uni-heidelberg.de), miRDB (http://mirdb.org), TargetScan (http://www.targetscan.org/vert_72/), Encori (http://starbase.sysu.edu.cn), and differentially expressed genes to predict target genes of miR-330-3p. We drew the ceRNA network using Cytoscape software.

GSEA

Gene expression of BC samples downloaded from the TCGA database (https://www.cancer.gov/about-nci/organization/ccg/research/structural-genomics/tcga) were divided into a high-level group and a low-level group according to the expression level of RAI2. The h.all.v7.0.symbols.gmt[Hallmark] dataset was downloaded from the Molecular Signatures Database (MSigDB) and was analyzed by GSEA 4.0.3 (https://www.broad.mit.edu/gsea/). Enrichment analysis was carried out according to the methods of default weighted enrichment statistics, and the analysis was repeated randomly 1,000 times at a time. NOM p <0.05, NES >1, and false discovery rate [FDR] q <0.25 were chosen as significance cutoff criteria.

Cell transfection and vector construction

Lipofectamine 2000 (Invitrogen, USA) was used to transfect small interfering RNA (siRNA) and miRNA mimics and inhibitors (GenePharma, Shanghai, China) into cells. To construct the overexpression plasmid, the sequence of circRBPMS was cloned into the plenti-ciR-GFP-T2A vector. The corresponding sequences were inserted into a pmirGLO vector (Promega, USA) to synthesize luc reporter plasmids. The miR-330-3p inhibitors and miR-330-3p mimics were purchased from GenePharma (Shanghai, China). Three shRNA molecules were designed to target transcripts of RAI2 and constructed into the pGPU6/GFP/puromycin vector: shRNA-1 (5′-GCTGTGCTCCAGAATTTGTTT-3′), shRNA-2 (5′-GCCACACGGTCATTAAGATGG-3′), and shRNA-3 (5′-GGGAAGAGTCCATGGGAAATG-3′).

Cell proliferation assays

For the CCK-8 assay, we placed T24 and UM-UC-3 cells into plates with 96 wells at a density of 1,500 cells per well. We detect cell viability 0, 24, 48, and 72 h after seeding into the wells according to the manufacturer's instructions.

For the colony formation assay, transfected cells were seeded into 6-well plates at a density of 600 cells/well and maintained for 8 days in DMEM containing 10% FBS. The colonies were imaged and counted after they were fixed and stained.

Apoptosis assay

Cell apoptosis was detected using the Annexin V-APC/7-AAD apoptosis kit (MultiSciences, AP105-100), following the manufacturer's instructions. Briefly, cells were incubated in APC Annexin-V and 7-AAD staining solution for 20 min at room temperature in the dark after washing in PBS. After incubation, cells were analyzed using a BD Accuri C6 flow cytometer and analyzed using FlowJo 10.0.7 software. Apoptotic cells were defined as the population of cells that were APC Annexin-V+ and 7-AAD− (undergoing apoptosis) or APC Annexin-V+ and 7-AAD+ (end of apoptosis or dead).

EdU assay

We utilized an EdU assay kit (RiboBio, China) to detect DNA synthesis and cell proliferation; 3,000 treated PC cells were seeded in a 96-well plate for one night. The next day, we added EdU solution (10 μM) to the 96-well plate and waited 24 h. Then we applied 4% formalin to fix the PC cells at room temperature for 2 h while other procedures following the manufacturer's protocol. A microscope (Nikon, Japan) was used to observe DNA synthesis and cell proliferation, reflected by red and blue signals, respectively.

Cell migration and invasion assays

For the wound healing assay, we placed T24 and UM-UC-3 cells into plates with 6 wells at a density of 20,000 cells per well. A wound was made using a 1,000-μL pipette tip, and we detected cell migration at 0, 12, 24, 48, and 72 h.

As for the Transwell assay, we used a BD Transwell chamber with 24 wells (Costar, Boston, MA, USA) according to the manufacturer's guidelines. Cells at a density of 60,000 in 500 μL serum-free medium were added to the upper chambers, and medium supplemented with 10% FBS was added to the lower chambers. After 24 h in a 37°C incubator, we used formaldehyde fixing and 1% crystal violet staining to visualize the migrated and invaded cells and calculated and photographed them.

Western blot analysis

We extracted protein from cells lysed in ice-cold RIPA lysis buffer and separated them using 10% SDS-PAGE. After blocking in 5% non-fat milk for 1 h, the membranes were incubated with RAI2 (Abcam, ab247100), E-Cadherin (Abcam, ab15148), Vimentin (Proteintech, 10366-1-AP), p-ERK (Cell Signaling Technology, 4370), ERK (CST, 4695), Myf5 (Abcam, ab125078), MyoG (Proteintech, 67082-1-lg), GADD45A (Abcam, ab180768), and GAL1 (Proteintech, 11858-1-AP). GAPDH (Proteintech, 60004-1-lg) was detected as an endogenous control. A horseradish peroxidase (HRP)-conjugated secondary antibody (Jackson ImmunoResearch Laboratories, USA) was next applied for 1 h at room temperature. Signals were visualized with an enhanced chemiluminescence (ECL) kit (CLiNX, Shanghai) and captured using an ECL imaging system (CLiNX, Shanghai). The optical density of the protein bands was quantified by ImageJ software 1.48 (National Institutes of Health, Bethesda, MD, USA)

RNA pull-down assay

Streptavidin-coupled magnetic beads (Life Technologies, USA) were incubated with the biotin-coupled circRBPMS probes above and oligo probes for 3 h at room temperature to generate probe-coated beads.[9] Approximately 1 × 107 BC cells were collected and sonicated, and cell lysates were incubated with probe-coated beads at 4°C overnight for further validation.

RIP assay

The RIP assay was performed using a magnetic RIP RNA-binding protein immunoprecipitation kit (Millipore). Cells were harvested and lysed in lysis buffer according to the manufacturer's instructions. The cell lysate was incubated at 4°C overnight with magnetic beads conjugated with an antibody against IgG or Ago2 (CST, 2897S). After washing twice with wash buffer, the RNA binding to beads was purified using RNA extraction reagent,[45] and the relative enrichment abundance of circRBPMS and miR-330-3p was detected by qRT-PCR.

Luc reporter assay

The WT cDNA fragments of circRBPMS or the RAI2 3′ UTR containing the predicted miR-330-3p binding sites and their mutant variant were cloned into the pmirGLO plasmid (Promega, Madison, WI, USA), respectively. For the luc reporter assay, HEK293T cells were co-transfected with the WT vector or Mut vector and miR-330-30 mimics or control mimics using Lipofectamine 2000 (Thermo Fisher Scientific). After 48 h of co-transfection, luc activity was detected using a dual-luc reporter assay kit (Promega), and relative *Renilla* luc (Rluc) activity was normalized. Each experiment was performed in triplicate.

Xenograft formation

All animals were purchased from SLARC (Shanghai, China) and approved by the Ethics Committee of Huashan Hospital, Fudan University, Shanghai, China. The mice were divided randomly into two groups (n = 6). A total of 2 × 107 viable NC LV-NC or LV-circRBPMS T24 cells were injected into the right flanks of nude mice. Tumor sizes were measured every 5 days using a Vernier caliper, and the volume was calculated using the following formula: volume = 1/2 × length × width^2. The mice were euthanized for further analyses 21 days after implantation.

For analysis of metastasis, T24 cells were transfected with luc expression vectors into LV-NC and LV-circRBPMS T24 cells (2 × 10^5), and then the cells were injected intravenously into the tails of 6 randomly divided mice. After 30 days, metastasis of T24 cells was analyzed by bioluminescence imaging with intravenous injection of luciferin (150 mg luciferin/kg body weight) into the mouse tails.

Immunohistochemistry

Tumor tissue samples were embedded in paraffin. Sections (5 mm thick) were stained with Ki67 to evaluate proliferation. Sections were examined using an Axiophot light microscope (Carl Zeiss, Oberkochen, Germany) and photographed with a digital camera.

Statistical analysis

Data are presented as mean ± SD (standard deviation). GraphPad Prism (GraphPad, La Jolla, CA, USA) was used to calculate group differences. The association between circRBPMS expression levels and clinical parameters was evaluated by chi-square test. Kaplan-Meier curves and log rank tests were applied for overall survival analysis. $p \leq 0.05$ was considered statistically significant.

SUPPLEMENTAL INFORMATION

Supplemental Information can be found online at https://doi.org/10.1016/j.omtn.2021.01.009.

ACKNOWLEDGMENTS

This work was supported by a clinical research and training project (SHDC12017X10) provided by the Shanghai Shen Kang Hospital Development Center and the National Natural Science Foundation of China (81802569).

AUTHOR CONTRIBUTIONS

C.Y. and H.J. designed the study. C.Y., Z.M., Z.Z., and Q.Z. performed the assays. X.C., X.D., and J.G. collected samples. C.X., Y.C., S.W., and Y.O. performed statistical analyses. C.Y. and Z.M. wrote the paper. All authors read and approved the final manuscript.

DECLARATION OF INTERESTS

The authors declare no competing interests.

REFERENCES

1. Liu, X., Jiang, J., Yu, C., Wang, Y., Sun, Y., Tang, J., Chen, T., Bi, Y., Liu, Y., and Zhang, Z.J. (2019). Secular trends in incidence and mortality of bladder cancer in China, 1990-2017: A joinpoint and age-period-cohort analysis. Cancer Epidemiol. *61*, 95–103.
2. Cong, L., Yang, Q., Hu, C., Yu, Q., Hao, S., and Li, D. (2019). Current Status of Functional Studies on Circular RNAs in Bladder Cancer and their Potential Role as Diagnostic and Prognostic Biomarkers: A Review. Med. Sci. Monit. *25*, 3425–3434.
3. Sanger, H.L., Klotz, G., Riesner, D., Gross, H.J., and Kleinschmidt, A.K. (1976). Viroids are single-stranded covalently closed circular RNA molecules existing as highly base-paired rod-like structures. Proc. Natl. Acad. Sci. USA *73*, 3852–3856.
4. Ashwal-Fluss, R., Meyer, M., Pamudurti, N.R., Ivanov, A., Bartok, O., Hanan, M., Evantal, N., Memczak, S., Rajewsky, N., and Kadener, S. (2014). circRNA biogenesis competes with pre-mRNA splicing. Mol. Cell *56*, 55–66.
5. Suzuki, H., Zuo, Y., Wang, J., Zhang, M.Q., Malhotra, A., and Mayeda, A. (2006). Characterization of RNase R-digested cellular RNA source that consists of lariat and circular RNAs from pre-mRNA splicing. Nucleic Acids Res. *34*, e63.
6. Jeck, W.R., and Sharpless, N.E. (2014). Detecting and characterizing circular RNAs. Nat. Biotechnol. *32*, 453–461.
7. Memczak, S., Jens, M., Elefsinioti, A., Torti, F., Krueger, J., Rybak, A., Maier, L., Mackowiak, S.D., Gregersen, L.H., Munschauer, M., et al. (2013). Circular RNAs are a large class of animal RNAs with regulatory potency. Nature *495*, 333–338.
8. Tay, Y., Rinn, J., and Pandolfi, P.P. (2014). The multilayered complexity of ceRNA crosstalk and competition. Nature *505*, 344–352.
9. Liu, H., Bi, J., Dong, W., Yang, M., Shi, J., Jiang, N., Lin, T., and Huang, J. (2018). Invasion-related circular RNA circFNDC3B inhibits bladder cancer progression through the miR-1178-3p/G3BP2/SRC/FAK axis. Mol. Cancer *17*, 161.
10. Yang, C., Wu, S., Wu, X., Zhou, X., Jin, S., and Jiang, H. (2019). Silencing circular RNA UVRAG inhibits bladder cancer growth and metastasis by targeting the microRNA-223/fibroblast growth factor receptor 2 axis. Cancer Sci. *110*, 99–106.
11. Lee, R.C., Feinbaum, R.L., and Ambros, V. (1993). The C. elegans heterochronic gene lin-4 encodes small RNAs with antisense complementarity to lin-14. Cell *75*, 843–854.
12. Berindan-Neagoe, I., Monroig, Pdel.C., Pasculli, B., and Calin, G.A. (2014). MicroRNAome genome: a treasure for cancer diagnosis and therapy. CA Cancer J. Clin. *64*, 311–336.
13. Tay, Y., Zhang, J., Thomson, A.M., Lim, B., and Rigoutsos, I. (2008). MicroRNAs to Nanog, Oct4 and Sox2 coding regions modulate embryonic stem cell differentiation. Nature *455*, 1124–1128.
14. Shah, M.Y., Ferrajoli, A., Sood, A.K., Lopez-Berestein, G., and Calin, G.A. (2016). microRNA Therapeutics in Cancer - An Emerging Concept. EBioMedicine *12*, 34–42.
15. Su, Y., Feng, W., Shi, J., Chen, L., Huang, J., and Lin, T. (2020). circRIP2 accelerates bladder cancer progression via miR-1305/Tgf-β2/smad3 pathway. Mol. Cancer *19*, 23.
16. Su, Y., Zhong, G., Jiang, N., Huang, M., and Lin, T. (2018). Circular RNA, a novel marker for cancer determination (Review). Int. J. Mol. Med. *42*, 1786–1798.
17. Lee, Y.J., Lee, G.J., Yi, S.S., Heo, S.H., Park, C.R., Nam, H.S., Cho, M.K., and Lee, S.H. (2016). Cisplatin and resveratrol induce apoptosis and autophagy following oxidative stress in malignant mesothelioma cells. Food Chem. Toxicol. *97*, 96–107.
18. Liu, L., Wu, S.Q., Zhu, X., Xu, R., Ai, K., Zhang, L., and Zhao, X.K. (2019). Analysis of ceRNA network identifies prognostic circRNA biomarkers in bladder cancer. Neoplasma *66*, 736–745.
19. Huang, Y., Sun, H., Ma, X., Zeng, Y., Pan, Y., Yu, D., Liu, Z., and Xiang, Y. (2020). HLA-F-AS1/miR-330-3p/PFN1 axis promotes colorectal cancer progression. Life Sci. *254*, 117180.
20. Wei, C., Zhang, R., Cai, Q., Gao, X., Tong, F., Dong, J., Hu, Y., Wu, G., and Dong, X. (2019). MicroRNA-330-3p promotes brain metastasis and epithelial-mesenchymal transition via GRIA3 in non-small cell lung cancer. Aging (Albany NY) *11*, 6734–6761.
21. Zheng, Z., Bao, F., Chen, X., Huang, H., and Zhang, X. (2018). MicroRNA-330-3p Expression Indicates Good Prognosis and Suppresses Cell Proliferation by Targeting Bmi-1 in Osteosarcoma. Cell. Physiol. Biochem. *46*, 442–450.
22. Zhao, X., Chen, G.Q., and Cao, G.M. (2019). Abnormal expression and mechanism of miR-330-3p/BTG1 axis in hepatocellular carcinoma. Eur. Rev. Med. Pharmacol. Sci. *23*, 6888–6898.
23. Esposito, M., and Kang, Y. (2015). RAI2: Linking Retinoic Acid Signaling with Metastasis Suppression. Cancer Discov. *5*, 466–468.
24. Xiao, M.S., Ai, Y., and Wilusz, J.E. (2020). Biogenesis and Functions of Circular RNAs Come into Focus. Trends Cell Biol. *30*, 226–240.
25. Li, Y., Zheng, F., Xiao, X., Xie, F., Tao, D., Huang, C., Liu, D., Wang, M., Wang, L., Zeng, F., and Jiang, G. (2017). CircHIPK3 sponges miR-558 to suppress heparanase expression in bladder cancer cells. EMBO Rep. *18*, 1646–1659.
26. Legnini, I., Di Timoteo, G., Rossi, F., Morlando, M., Briganti, F., Sthandier, O., Fatica, A., Santini, T., Andronache, A., Wade, M., et al. (2017). Circ-ZNF609 Is a Circular RNA that Can Be Translated and Functions in Myogenesis. Mol. Cell *66*, 22–37.e9.
27. Guo, J.U., Agarwal, V., Guo, H., and Bartel, D.P. (2014). Expanded identification and characterization of mammalian circular RNAs. Genome Biol. *15*, 409.
28. Gomes, C.P.C., Salgado-Somoza, A., Creemers, E.E., Dieterich, C., Lustrek, M., and Devaux, Y.; Cardiolinc™ network (2018). Circular RNAs in the cardiovascular system. Noncoding RNA Res. *3*, 1–11.
29. Wang, X., Tan, L., Lu, Y., Peng, J., Zhu, Y., Zhang, Y., and Sun, Z. (2015). MicroRNA-138 promotes tau phosphorylation by targeting retinoic acid receptor alpha. FEBS Lett. *589*, 726–729.
30. Mooers, B.H., Logue, J.S., and Berglund, J.A. (2005). The structural basis of myotonic dystrophy from the crystal structure of CUG repeats. Proc. Natl. Acad. Sci. USA *102*, 16626–16631.
31. Mao, W., Huang, X., Wang, L., Zhang, Z., Liu, M., Li, Y., Luo, M., Yao, X., Fan, J., and Geng, J. (2019). Circular RNA hsa_circ_0068871 regulates FGFR3 expression and activates STAT3 by targeting miR-181a-5p to promote bladder cancer progression. J. Exp. Clin. Cancer Res. *38*, 169.
32. Liu, P., Li, X., Guo, X., Chen, J., Li, C., Chen, M., Liu, L., Zhang, X., and Zu, X. (2019). Circular RNA DOCK1 promotes bladder carcinoma progression via modulating circDOCK1/hsa-miR-132-3p/Sox5 signalling pathway. Cell Prolif. *52*, e12614.
33. Bi, J., Liu, H., Dong, W., Xie, W., He, Q., Cai, Z., Huang, J., and Lin, T. (2019). Circular RNA circ-ZKSCAN1 inhibits bladder cancer progression through miR-1178-3p/p21 axis and acts as a prognostic factor of recurrence. Mol. Cancer *18*, 133.
34. Xiao, W., Adhikari, S., Dahal, U., Chen, Y.S., Hao, Y.J., Sun, B.F., Sun, H.Y., Li, A., Ping, X.L., Lai, W.Y., et al. (2016). Nuclear m(6)A Reader YTHDC1 Regulates mRNA Splicing. Mol. Cell *61*, 507–519.
35. Yu, C.Y., Li, T.C., Wu, Y.Y., Yeh, C.H., Chiang, W., Chuang, C.Y., and Kuo, H.C. (2017). The circular RNA circBIRC6 participates in the molecular circuitry controlling human pluripotency. Nat. Commun. *8*, 1149.
36. Abdelmohsen, K., Panda, A.C., Munk, R., Grammatikakis, I., Dudekula, D.B., De, S., Kim, J., Noh, J.H., Kim, K.M., Martindale, J.L., and Gorospe, M. (2017). Identification of HuR target circular RNAs uncovers suppression of PABPN1 translation by CircPABPN1. RNA Biol. *14*, 361–369.

37. Xu, X., Zhang, J., Tian, Y., Gao, Y., Dong, X., Chen, W., Yuan, X., Yin, W., Xu, J., Chen, K., et al. (2020). CircRNA inhibits DNA damage repair by interacting with host gene. Mol. Cancer *19*, 128.

38. Zang, J., Lu, D., and Xu, A. (2020). The interaction of circRNAs and RNA binding proteins: An important part of circRNA maintenance and function. J. Neurosci. Res. *98*, 87–97.

39. Jin, Z., Jia, B., Tan, L., and Liu, Y. (2019). miR-330-3p suppresses liver cancer cell migration by targeting MAP2K1. Oncol. Lett. *18*, 314–320.

40. Wang, Z., Qu, H., Gong, W., and Liu, A. (2018). Up-regulation and tumor-promoting role of SPHK1 were attenuated by miR-330-3p in gastric cancer. IUBMB Life *70*, 1164–1176.

41. Mesci, A., Huang, X., Taeb, S., Jahangiri, S., Kim, Y., Fokas, E., Bruce, J., Leong, H.S., and Liu, S.K. (2017). Targeting of CCBE1 by miR-330-3p in human breast cancer promotes metastasis. Br. J. Cancer *116*, 1350–1357.

42. Yan, W., Wu, K., Herman, J.G., Xu, X., Yang, Y., Dai, G., and Guo, M. (2018). Retinoic acid-induced 2 (RAI2) is a novel tumor suppressor, and promoter region methylation of RAI2 is a poor prognostic marker in colorectal cancer. Clin. Epigenetics *10*, 69.

43. Werner, S., Brors, B., Eick, J., Marques, E., Pogenberg, V., Parret, A., Kemming, D., Wood, A.W., Edgren, H., Neubauer, H., et al. (2015). Suppression of early hematogenous dissemination of human breast cancer cells to bone marrow by retinoic Acid-induced 2. Cancer Discov. *5*, 506–519.

44. Pastushenko, I., and Blanpain, C. (2019). EMT Transition States during Tumor Progression and Metastasis. Trends Cell Biol. *29*, 212–226.

45. Yue, B., Wang, J., Ru, W., Wu, J., Cao, X., Yang, H., Huang, Y., Lan, X., Lei, C., Huang, B., and Chen, H. (2020). The Circular RNA circHUWE1 Sponges the miR-29b-AKT3 Axis to Regulate Myoblast Development. Mol. Ther. Nucleic Acids *19*, 1086–1097.